Targeting DNA-LNPs to Endothelial Cells Improves Expression Magnitude, Duration, and Specificity

Nicolas Marzolini[1]*, Taylor V. Brysgel[2]*, Eno-Obong Essien[3], Ryan J. Rahman[4], Jichuan Wu[3], Aparajeeta Majumder[2], Manthan N. Patel[2], Sachchidanand Tiwari[3], Carolann L. Espy[2], Vladimir V. Shuvaev[2], Elizabeth D. Hood[2], Liam S. Chase[1], Jeremy B. Katzen[2,5], David B. Frank[5], Mariko L. Bennett[4,6], Oscar A. Marcos Contreras[2,3], Jacob W. Myerson[1,2], Vladimir R. Muzykantov[2]**, Sahily Reyes-Esteves[4]**, Jacob S. Brenner[2,3]**

Affiliations:

1) Department of Bioengineering, University of Pennsylvania, Philadelphia, PA 19104, USA
2) Department of Systems Pharmacology and Translational Therapeutics, Perelman School of Medicine, University of Pennsylvania, Philadelphia, PA 19104, USA
3) Division of Pulmonary Allergy, and Critical Care, Department of Medicine, Perelman School of Medicine, University of Pennsylvania, Philadelphia, PA 19104, USA
4) Department of Neurology, Perelman School of Medicine, University of Pennsylvania, Philadelphia, PA, 19104, USA
5) Penn-CHOP Lung Biology Institute, Perelman School of Medicine, University of Pennsylvania, Philadelphia, PA 19104, USA
6) Division of Neurology, Children's Hospital of Philadelphia, Philadelphia, PA 19104, USA

*Denotes Equal Contribution
**Co-Corresponding Authors
Co-Corresponding Author Emails:
Jacob Brenner: Jacob.Brenner@pennmedicine.upenn.edu
Sahily Reyes-Esteves: Sahily.Reyes-Esteves@pennmedicine.upenn.edu
Vladimir R. Muzykantov: muzykant@pennmedicine.upenn.edu

Keywords: Drug Delivery Systems; Nanoparticles; Endothelium; Drug Targeting; DNA

Table of Contents: Attaching antibodies against endothelial cell surface proteins redirects the delivery and expression of DNA-lipid nanoparticles to organs of interest. Our targeted nanoparticles enable organ-selective DNA expression in the endothelium of the lungs, brain, or spleen, providing a therapeutic platform for dozens of endothelial-centric diseases.

Abstract

DNA-lipid nanoparticles (DNA-LNPs) loaded with inhibitors of the cGAS-STING pathway enable safe and effective delivery of DNA *in vivo*. However, unmodified LNPs primarily accumulate in the liver. Herein, we report the first instances of extrahepatic DNA-LNP targeting, focused on delivery to endothelial cells, as they play a central role in myriad diseases, such as pulmonary hypertension and stroke. DNA-LNPs conjugated to antibodies against PECAM-1 or VCAM-1 target the endothelium of the lungs and brain/spleen, respectively. These LNPs drive robust transgene expression in their target organs, with greater magnitude and duration than untargeted LNPs. Organ specificity of PECAM-targeted expression increases markedly over two weeks, as off-target liver expression declines to undetectable levels. This improvement in organ-specificity of expression is further improved by replacing full-length antibodies with Fab fragments, resulting in a markedly higher lung-to-liver expression ratio than mAb mRNA-LNPs. Single-cell expression analysis reveals the mechanism underlying the improvements in organ-specificity: target organ expression is dominated by long-lived endothelial cells, while off-target liver expression is in non-endothelial cells with shorter half-lives. Collectively, these studies demonstrate that targeted DNA-LNPs achieve high levels of organ- and cell-type-specific transgene expression and thus provide a therapeutic platform for dozens of endothelial-centric diseases.

1. Introduction

Lipid nanoparticles (LNPs) are a versatile delivery system with immense therapeutic potential due to their ability to encapsulate nucleic acid therapies[1]. In the past, LNPs have traditionally been loaded with messenger RNA (mRNA), as in the COVID-19 vaccines, to express encoded proteins as therapies or antigens[2]. LNPs loaded with small interfering RNAs (siRNAs) to silence gene expression have also seen therapeutic success, as Patisiran was the first FDA-approved lipid nanoparticle[3]. Despite these accomplishments, RNA-LNPs have not yet been clinically translated for chronic indications due to the relatively short half-life of RNA[1]. For this purpose, DNA-LNPs are an attractive drug delivery system based on their potential for long-term expression, less frequent dosing, and enhanced stability[4].

Historically, DNA-LNPs have been too inflammatory to use *in vivo*, as the delivery of DNA to the cytosol activates the stimulator of interferon genes (STING) signaling pathway, leading to the upregulation of pro-inflammatory cytokines and type 1 interferons that induce 100% mortality at biologically relevant doses[4-6]. Our lab has recently published methods to reduce this inflammation by co-loading DNA-LNPs with 9(10)-nitrooleic acid (NOA), a lipid inhibitor of the STING pathway[7]. These NOA-DNA-LNPs significantly alleviate inflammation *in vivo* and reduce mortality to 0% at doses up to 25µg of plasmid DNA (pDNA) loaded into bare (unconjugated) LNPs[6]. Further, NOA-DNA-LNPs express > 6 months per dose, have much larger cargo capacity than the dominant viral vector (adeno-associated virus, or AAV), and can be redosed[8,9]. With these characteristics, DNA-LNPs are poised to fill niches in gene therapy which cannot be served by AAVs, such as delivery of large transgenes, delivery to patients with AAV antibodies, and treatment of common chronic diseases (*e.g.*, atherosclerosis, osteoarthritis, etc.)[10,11].

When administered intravenously (IV), most unmodified LNPs, whether carrying DNA or RNA, accumulate predominantly in the liver[12]. This makes it difficult to use LNPs to treat most diseases outside the liver. Therefore, we started the campaign to target DNA-LNPs to specific organs and cell types. As our first target, we chose endothelial cells, for two reasons. First, endothelial cells play a central role in many illnesses, including pulmonary hypertension (PH) and stroke[13,14]. Second, if we can target DNA-LNPs to capillary endothelial cells in a specific organ, we could turn those cells into biofactories which secrete therapeutic proteins into the parenchyma of that organ, a strategy that could treat many diseases that are not endothelial-centric[15].

Historically, two approaches to achieve targeted delivery of LNPs to the endothelium have been implemented: (1) attaching affinity ligands, such as antibodies against cell-specific targets, to their surfaces or (2) modifying the physical or chemical features of the LNP, such as introducing permanently cationic lipids like 1,2-dioleoyl-3-trimethylammonium propane (DOTAP) into the formulation[16-19]. However, physicochemical tropism has been shown to induce severe toxicities in vivo (*e.g.*, thrombosis)[20]. We thus utilize affinity targeting of endothelial cell surface proteins. Platelet endothelial cell adhesion molecule 1 (PECAM-1) is an attractive candidate for redirecting the delivery of LNPs to the lungs, since it is highly expressed on the surface of pulmonary endothelial cells[21]. Moreover, the lungs receive the entire cardiac output and have a large vascular surface area[22]. Conjugating anti-PECAM-1 (αPECAM) antibodies to the surface of mRNA-LNPs has been shown to redirect their delivery to the lungs, achieving ~100% injected dose per gram tissue (%ID/g)[23]. Similarly, conjugating antibodies against vascular cell adhesion molecule 1 (VCAM-1), another adhesion molecule whose

expression is upregulated in inflammatory conditions, increases the delivery and expression of targeted nanocarriers to the endothelium of the spleen and brain[24-28].

Here, we adapt this strategy for NOA-DNA-LNPs (referred to as DNA-LNPs, hereafter) to target them to the endothelium of different organs. By conjugating monoclonal antibodies (mAbs) against PECAM-1or VCAM-1 to nanoparticles, we redirect their delivery and expression to the lungs and spleen/brain, respectively. *Ex vivo* imaging of organ luminescence confirms this DNA expression as being concentrated in the target organs and demonstrates that the lung versus liver specificity of our targeted DNA-LNP expression increases over time. Replacing full-length PECAM mAbs with fragment-antigen binding regions (Fabs) increases the magnitude, longevity, and organ-type specificity of transgene expression. Using flow cytometry and immunofluorescence, we identify pulmonary endothelial cells as the primary cell type targeted by our αPECAM-Fab nanoparticles and responsible for transgene expression. Overall, these results highlight the immense potential of targeted DNA-LNPs for treating a variety of endothelial pathologies.

2. Results

2.1. Conjugating αPECAM antibodies to DNA-LNPs redirects their delivery to the lungs

We first fabricated DNA-LNPs based on Pfizer-BioNTech's FDA-approved COVID-19 mRNA vaccine LNP formulation, which consists of the ionizable lipid ALC-0315, the phospholipid 1,2-distearoyl-sn-glycero-3-phosphocholine (DSPC), cholesterol, and ALC-0159, which was replaced fully with 1,2-distearoyl-sn-glycero-3-phosphoethanolamine -N-[azido(polyethylene glycol)-2000] (DSPE-PEG(2000)-Azide)[29]. Our LNPs were loaded with reporter plasmid DNA encoding for either luciferase, mCherry, or Cre recombinase (lipid/pDNA ratio of 40/1, wt/wt) (**Figure 1A**). The replacement of ALC-0159 with DSPE-PEG(2000)-Azide allowed us to conjugate antibodies to the surface of LNPs using established click chemistry methods[26,30]. Additionally, we co-loaded NOA into our lipid formulation, which inhibits the cytosolic DNA sensor, STING, thereby reducing inflammation and mitigating mortality as described in our prior work[4-6]. αPECAM monoclonal antibodies conjugated to DNA-LNPs with greater than 80% conjugation efficiency (**Figure S1)**, resulting in average size increases of 15-20nm post-conjugation and polydispersity indices (PDIs) consistently < 0.2 (**Figure 1B**).

For biodistribution studies, we intravenously injected naive, BALB/c mice with either (1) DNA-LNPs conjugated to αPECAM mAbs (~50 per particle) and radiolabeled immunoglobulin G (IgG, 5 mAbs per particle) or (2) DNA-LNPs conjugated to untargeted IgG and radiolabeled IgG (50 IgG mAbs, 5 radiolabeled IgG mAbs per particle). Each mouse was dosed by total injected radioactivity in counts per minute (cpm) that equated to ~2.5μg of pDNA. 30 minutes after injection, all mice were euthanized to determine the organ distribution of the particles. αPECAM DNA-LNPs accumulated in the lungs markedly better than untargeted IgG DNA-LNP controls, with a percent injected dose per gram of tissue (%ID/g) of ~90% (**Figure 1C**), underscoring that targeting PECAM-1 effectively redirects the delivery of LNPs to the lungs. Notably, αPECAM DNA-LNPs had no significant difference in delivery to any organ other than the lungs, although delivery to the liver downtrends (**Figure 1E**). The localization ratio of αPECAM DNA-LNPs, which accounts for blood retention, is normalized tissue %ID/g divided by %ID/g found in whole blood, was ~35x higher than IgG controls (**Figure 1D**). We also tested additional formulations of αPECAM DNA-LNPs using the ionizable lipid SM-102 and the phospholipid 1,2-Dioleoyl-sn-glycero-3-phosphoethanolamine (DOPE). While these alternative

DNA-LNPs targeted the lungs similarly, our initial ALC-0315/DSPC formulation exhibited the highest conjugation efficiency to αPECAM mAbs (**Figure S1**) and matched the highest levels of lung targeting (**Figure S2**). Accordingly, our studies in the remainder of this paper utilize this LNP formulation.

2.2 αPECAM DNA-LNPs express in the lungs *in vivo*

We next investigated the transgene expression of our targeted αPECAM DNA-LNPs by measuring both *in vivo* and *ex vivo* luminescence. Initially, two doses were tested in naïve mice with either 2.5 or 5μg of luciferase DNA loaded into LNPs conjugated to αPECAM mAbs. The magnitude of *in vivo* luciferase expression in the thoracic cavity of the mice was measured using an in vivo imaging system (IVIS), which quantifies luminescence following intraperitoneal (IP) administration of the luciferase substrate, luciferin. One day following injection, luminescence in the αPECAM DNA-LNP-treated mice was visibly concentrated in the thorax, with highest levels of signal appearing to emit from the lungs (**Figure 2A, S3**). Total mean luminescence of mice treated with 5μg of pDNA reached a peak of ~5 x 10^6 photons s^{-1} at day 1, before steadily declining and plateauing around 7 x 10^5 photons s^{-1} by day 7, which was stable at day 14, after which animals were euthanized for *ex vivo* analysis (**Figure 2B**). The day 14 luminescence in mice treated with αPECAM DNA-LNPs was significantly higher than that from untreated control mice (~10^5 photons s^{-1}). Untargeted IgG DNA-LNP controls (5μg pDNA) quickly plateaued by day 3, maintaining luminescence ~2x greater than untreated controls thereafter (**Figure S4)**. Furthermore, luminescence from mice treated with 5μg of pDNA loaded in αPECAM DNA-LNPs was higher than mice treated with 2.5μg of pDNA, whose signal was also concentrated in the lungs (**Figure S3**) and followed a similar trend of peaking within the first few days and plateauing by day 7 (**Figure 2B**).

To confirm that our observed luminescence was predominantly in the lungs, we IV treated mice with 5μg of pDNA loaded into PECAM-targeted or untargeted IgG DNA-LNPs. At either 1 or 14 days after treatment, mice were euthanized to measure the total flux of *ex vivo* luminescence of individual organs via IVIS (quantification method provided in **Figure S5**). At both days 1 and 14, the majority of luminescence emitted from the lungs, with a drop in luminescence from ~8 x 10^5 photons s^{-1} at day 1 to ~5 x 10^5 photons s^{-1} at day 14 (**Figures 2C, 2E, 2F**). This was significantly higher than the lung expression measured from IgG DNA-LNPs and untreated control mice, both of which emitted luminescence below 10^4 photons s^{-1} at 1d. Given the sharp decline of total *in vivo* IgG DNA-LNP luminescence to a mere ~2x background by day 3, *ex vivo* quantifications at day 14 were not performed.

Surprisingly, our *ex vivo* quantifications revealed considerable decrease in liver luminescence in mice treated with αPECAM DNA-LNPs over the 14 day period, dropping a full order of magnitude by day 14. This decrease in liver signal is significantly larger than the concurrent decrease in lung signal. Thus, the specificity of our αPECAM DNA-LNP lung expression increases over time, with a nearly 5-fold increase in the quantified lung:liver expression ratio over 14 days (**Figure 2D**).

2.3 Targeting VCAM-1 redirects the delivery and expression of DNA-LNPs to the spleen and brain

In order to show the generalizability of our platform, we swapped the targeting antibody from αPECAM to anti-VCAM-1 (αVCAM) mAbs. VCAM-1 is a cell adhesion molecule, similar to PECAM-1, whose expression is highly upregulated during pathological conditions[24]. Previous

studies have shown that drug delivery systems targeting VCAM-1 accumulate in the spleen[26,31]. However, αVCAM nanocarriers also experience a significant increase in brain uptake compared to controls[25,27,28]. Our results similarly show that radiolabeled, IV-administered αVCAM DNA-LNPs (50 mAbs per particle) accumulate in the spleen of naive mice 30 minutes after injection at ~85 %ID/g (**Figure 3A**). This was significantly more than αPECAM and untargeted IgG DNA-LNPs, which both have a %ID/g of ~50% in the spleen. αVCAM DNA-LNPs also targeted the brain >3 times better than both αPECAM and untargeted IgG nanoparticles (**Figure 3D**).

To quantify the expression of VCAM-targeted nanoparticles, we again IV-treated mice with 5μg of luciferase pDNA loaded into αVCAM DNA-LNPs and measured *ex vivo* luminescence of individual organs via IVIS 1 day following treatment. At this time and dose, we only observed elevated luminescence in the spleen at ~2 x 10^5 photons s^{-1}, which was significantly higher than naive, luciferin-treated control mice (**Figure 3C-D**). We did not detect luminescence in the brain, which is expected given (1) the relatively low dose of pDNA and (2) the detection sensitivity of IVIS for organs with lower nanoparticle uptake.

To show that our αVCAM DNA-LNPs express in the brain, we used immunofluorescence (IF). Ai6 mice, which express an enhanced green fluorescent protein (ZsGreen) following Cre-mediated recombination of a STOP cassette, were intravenously injected with αVCAM DNA-LNPs loaded with 5μg of pDNA encoding Cre recombinase (**Figure 3E**). 24 hours after treatment, brains were harvested and stained with DAPI and fluorescent antibodies against PECAM-1 (CD31) (**Figure 3F**). Our images show expression of ZsGreen either colocalized with or adjacent to endothelial cells, shown in a representative confocal image of a brain blood vessel (**Figure 3G**).

Similarly, we repeated IF using αVCAM DNA-LNPs loaded with mCherry pDNA, encoding a red monomeric fluorescent protein, 4 hours post-injection in naive BALB/c mice. This alternate approach also shows expression observed within the neurovasculature, which is significant as mCherry is a true transgene as opposed to the constitutive expression of Cre-induced ZsGreen in Ai6 mice (**Figure 3H, Figure S6**). These images confirm that αVCAM DNA-LNPs target and express in different regions of the brain endothelium as early as 4 hours post-treatment. Taken together, these findings highlight the robustness of antibody targeting and its potential as a drug delivery system for both the spleen and CNS.

2.4 Fabs improve the delivery, expression, and specificity of lung targeted DNA-LNPs

We repeated prior experiments with αPECAM Fabs conjugated to our DNA-LNPs rather than mAbs. Fabs are the antigen-binding fragments of full-length antibodies, are smaller than mAbs (50 kDa vs 150 kDa), and lack a fragment crystallizable (Fc) region, which is the portion of the antibody that interacts with cell surface receptors on immune and other cell types[32-34] **(Figure 4A)**. We hypothesized that Fabs would improve the specificity of αPECAM DNA-LNPs by eliminating Fc-mediated interactions of the LNPs with targets other than PECAM. αPECAM Fabs conjugated to DNA-LNPs as well as mAbs, with a conjugation efficiency of >80% (**Figure S1**). Fabs were added to DNA-LNPs at a concentration of 100 Fabs per particle, in order to match the number of binding domains on the LNPs with 50 mAbs/particle tested above (**Figure 4A)**. Radiolabeled αPECAM-Fab DNA-LNPs targeted the lungs of naive mice at ~80% ID/g 30 minutes after IV treatment, matching mAb-conjugated nanoparticles (**Figure 4B**).

Once again, we used IVIS to investigate *in vivo* transgene expression of αPECAM-Fab DNA-LNPs loaded with 5μg of luciferase pDNA. One day after IV injection in naive mice, luminescence was concentrated in the thoracic cavity, with the majority of the signal emitting

from the lungs, visibly outlining the organ (**Figure 4C**). This is confirmed by *ex vivo* analysis of individual organs 1 day post-treatment, which clearly demonstrates that the majority of signal originates from the lungs, with low-level luminescence in the liver and spleen (**Figure 4D**). The total flux of the overall *in vivo* luminescence in αPECAM-Fab DNA-LNP treated mice after one day was very similar to mAbs at ~5 x 10^6 photons s^{-1}, although Fab expression peaked slightly higher after 2 days at ~7 x 10^6 photons s^{-1} (**Figure 4E**). The duration of αPECAM-Fab DNA-LNP luminescence followed a nearly identical trend to mAbs, steadily declining until day 7 before plateauing at 10^6 photons s^{-1} from days 7-14.

Notable differences between Fab- and mAb-conjugated DNA-LNPs became more apparent when analyzing the transgene expression of *ex vivo* organs over time. 14 days post-injection, the lung luminescence in mice treated with αPECAM-Fab DNA-LNPs was nearly an order of magnitude higher than mAbs (**Figure 4F**). Moreover, the specificity of αPECAM-Fab DNA-LNP lung expression was vastly superior to mAbs, with their lung:liver expression ratio increasing from 27 at day 1 to 111 at day 14, compared to 5 at day 1 and 22 at day 14 for mAbs (**Figure 4G**).

To further visualize the expression of our αPECAM-Fab DNA-LNPs in the lungs, we performed immunofluorescence. Mice were IV-injected with αPECAM-Fab DNA-LNPs loaded with 5μg of pDNA encoding mCherry. Sections prepared from lungs 4 hours after treatment showed clear expression of mCherry in endothelial cells of the pulmonary vasculature (**Figure S6**). In totality, these findings emphasize that Fabs are the more specific, better expressing, and overall superior moiety for lung-targeted DNA-LNPs.

2.5 PECAM-targeted Fab DNA-LNPs primarily deliver to and express in pulmonary endothelial cells

To probe cell specificity of our optimized targeting formulation with αPECAM Fabs, we utilized flow cytometry to identify the cell types that our αPECAM-Fab DNA-LNPs are delivered to and ultimately expressed in. First, we formulated αPECAM-Fab DNA-LNPs with Alexa Fluor 488 (AF488) fluorescent lipid to track the cellular distribution and uptake of the nanoparticle. These LNPs were IV-injected into naive mice at a 5μg pDNA dose, and 30 minutes later the animals were sacrificed and perfused to prepare the lungs and liver into single cell suspensions. Antibody stains identified general immune cells (anti-CD45), monocytes and macrophages (anti-CD64), neutrophils (anti-Ly6G), endothelial cells (anti-CD31), and epithelial cells (anti-EpCAM) to determine which cells αPECAM-Fab DNA-LNPs were delivered to (**Figure S8**). Out of all the LNP+ cells in the lungs, 77% were endothelial, 13% were CD45+/CD64-/Ly6G- immune cells (labeled, “other immune cells”), and 3% were neutrophils (**Figure 5A, Left**). In the liver, LNPs were primarily delivered to CD45-/CD31-/EpCAM- cells (labeled, “other cells”) at 53%, followed by endothelial cells at 29%. The “other cells” in the liver are predominantly hepatocytes. This analysis illustrates that αPECAM-Fab DNA-LNPs are highly endothelial-specific, especially in the lungs.

Because LNP delivery does not always lead to transgene expression, we also utilized flow cytometry to detect the expression of αPECAM-Fab DNA-LNPs in the same cell populations. 5μg of mCherry pDNA were loaded into αPECAM-Fab DNA-LNPs and IV administered into naive mice. 1 day after treatment, the animals were sacrificed and perfused to prepare single cell suspensions for flow cytometry using the same parameters as before. 65% of mCherry expressing cells in the lungs were endothelial, followed by “other cells” at 19%. (**Figure 5A, Right**). In totality, 12% of all pulmonary endothelial cells recovered expressed

mCherry, which is higher than any other cell population (**Figure 5B**). In the liver, nearly all of the mCherry expressing cells were from the "other cells" population, at 98% (**Figure 5A, Right**). This reveals an interesting discrepancy, as αPECAM-Fab DNA-LNPs delivered well to ECs in the liver yet expressed poorly. While surprising, this phenomenon could be explained by differences in the endothelial cell expression phenotype between the liver and lungs. Our flow data supports this hypothesis, as our recovered population of pulmonary endothelial cells have a noticeable shift in mCherry expression compared to liver endothelial cells, and also have a significantly higher geometric mean fluorescence intensity (gMFI) (**Figures 5C-D).**

Overall, our flow data uncover a theory explaining why the lung specificity of αPECAM-Fab DNA-LNPs is superior to that of mAbs and increases over time. Fabs better evade recognition by the innate immune system due to their lack of an Fc domain[35,36] (**Figure 5E**). Therefore, αPECAM-Fab DNA-LNPs are less likely to be taken up by phagocytes expressing Fc receptors and subsequently sequestered to reservoirs of immune cells in the liver [37]. Instead, they exhibit superior binding and uptake by pulmonary endothelial cells, explaining why Fab-conjugated nanoparticles are more lung-specific than mAbs. This hypothesis also explains why lung specificity increases over time in general, as the half-lives of immune cells and other cells are significantly shorter than endothelial cells, which remain quiescent for years[38,39] (**Figure 5E**). Therefore, the expression of cells in the liver diminishes over the course of 14 days, while pulmonary endothelial cell expression persists[40].This means the effect of our αPECAM-Fab DNA-LNPs in the lungs, dominated by long-lived endothelial cells, will remain despite its reduction in other organs.

3. Discussion

While mRNA-LNP therapies have seen success for a few applications where transgene expression is meant to be short-lived, the hours-long half-life of mRNA limits clinical use in the treatment of chronic diseases. Furthermore, regardless of cargo, LNPs predominantly accumulate in the liver, limiting their therapeutic relevance in extrahepatic diseases. Thus, following our prior work mitigating the morbidity and mortality of DNA-LNPs by loading them with the STING inhibitor NOA, we sought to extend this platform by targeting our novel drug delivery system to various vascular beds, focusing primarily on the lungs. In doing so, we show effective, organ-specific transgene expression that underscores the potential for targeted DNA-LNP therapies in chronic lung and vascular diseases.

Using bioluminescence, we demonstrate that our αPECAM DNA-LNPs induce high transgene expression in the lungs that persists for weeks, with significant increases in lung versus liver specificity with time. Single-cell analysis confirmed that the vast majority of expression in the lungs was confined to target endothelial cells, which are more quiescent than other transfected cell types[38,39]. From these data, we can extract two main points: (1) PECAM targeting is a highly effective method to achieve lung delivery of DNA-LNPs, and (2) targeting DNA-LNPs to the vascular endothelium prolongs transgene expression by confining DNA delivery to cells that will not actively apoptose or divide. The corollary to this second point is that any organ whose endothelium is effectively targeted will express with higher specificity over time, as the DNA is either destroyed or diluted in other cell types that have shorter half-lives or undergo frequent divisions. Thus, endothelial cells provide the optimal target for lung delivery of DNA-LNPs.

We expanded on our finding by targeting the same PECAM-1 epitope with Fabs in place of mAbs. We hypothesized that removing the Fc region from mAbs would limit phagocytic uptake and complement opsonization of our LNPs[32-34]. Indeed, using Fabs improved both lung specificity and expression of our DNA-LNPs. We attribute this phenomenon to the superior endothelial targeting of αPECAM-Fab DNA-LNPs, as they are less visible to the body's innate immune mechanisms. Interestingly, the geometric mean fluorescent intensity of lung endothelial cells is more than triple that of liver endothelial cells, indicating fundamental differences in how the endothelial cells of various organs process DNA delivered by LNPs. Given the unique role that liver sinusoidal endothelial cells (LSECs) play in the clearance of blood-borne waste, they exhibit a highly endocytic and degradative phenotype[41,42]. This offers an explanation as to why LSECs avidly take up αPECAM DNA-LNPs but do not express their DNA cargo to the same extent as lung endothelial cells. These differences amongst endothelial cells are not explored any further herein and will need to be studied in future work.

Finally, we aimed to show the flexibility of our platform by swapping out the PECAM-1 targeting moiety with one against VCAM-1. αVCAM DNA-LNPs showed highly specific spleen expression and increased brain uptake compared with αPECAM and IgG DNA-LNPs. Although not shown here, VCAM-1 is heavily upregulated in the brain microvasculature during inflammatory states, which can greatly increase nanoparticle uptake[24-28]. When considering that chronic diseases are generally accompanied by global low-level inflammation, it is conceivable that VCAM-targeting would improve brain specificity and expression in chronic neurological disease models, warranting future use of our αVCAM DNA-LNPs in studies of brain diseases[43].

While this study achieves specific endothelial targeting of DNA-LNPs, additional work is needed to expand on our platform technology. Further studies distinguishing the various subtypes of endothelial cells transfected (e.g., arterial, capillary, venous) will determine the pathologies targeted in future preclinical work. For example, if pulmonary arterial endothelial cells are significantly transfected, we can adapt our platform to deliver therapeutics in disease models of pulmonary hypertension. Likewise, while our targeted DNA-LNPs target the organ of interest with high endothelial transfection, promoters could further enhance endothelial specificity—an advantage enabled by the inherent flexibility of DNA cargo. We envision that combining our targeted DNA-LNPs with advanced DNA engineering will enable us to leverage endothelial cells as biofactories that secrete therapeutics directly onto parenchymal cells.

Collectively, our study greatly expands the therapeutic prospects of DNA-LNPs to include chronic diseases of the lungs, spleen, and brain. Furthermore, we have shown that simply swapping targeting moieties is an effective tool to alter the biodistribution of DNA-LNPs and induce organ-specific transgene expression that invariably increases over time when targeting endothelial cells.

4. Figures

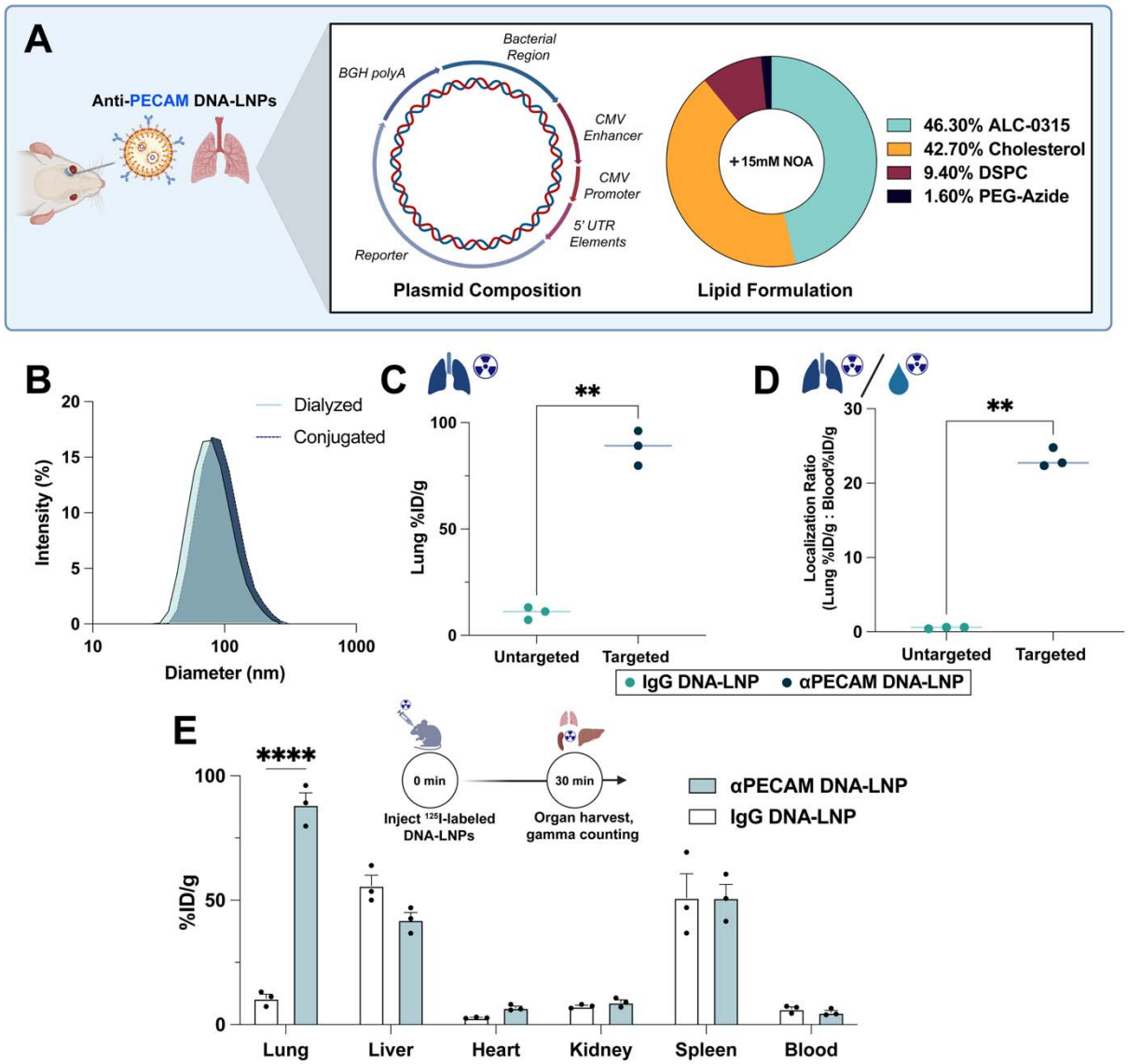

Figure 1. Anti-PECAM DNA-LNPs specifically target the lungs. (A) Graphical schematic depicting (left) treatment paradigm with retro-orbital injections of αPECAM DNA-LNPs with the illustrated lipid formulation and Nanoplasmid DNA. (B) DNA-LNP hydrodynamic diameter

distribution before and after conjugation with αPECAM monoclonal antibodies as determined by dynamic light scattering (DLS). (C) Biodistribution study via radiotracing of ^{125}I-labeled DNA-LNPs reveals ~9-fold increase in lung uptake of αPECAM DNA-LNPs compared to untargeted IgG DNA-LNPs. %ID/g represents the percent of total injected dose detected in each organ normalized by respective organ mass. (D) Localization ratios accounting for blood retention of DNA-LNPs display ~35x higher lung uptake of αPECAM DNA-LNPs compared with untargeted IgG controls when normalizing by blood signal. (E) Biodistribution of major abdominal and thoracic organs shows highest nanoparticle uptake in the lungs of mice administered αPECAM DNA-LNPs with no statistically significant difference in any other measured organ. For panels (C) and (D), unpaired *t*-tests with Welch's correction were performed. In panel (E), a two-way ANOVA with Tukey's multiple comparisons test was performed. All data include n = 3 and represent mean ± SEM; ** = $p < 0.01$, **** = $p < 0.0001$.

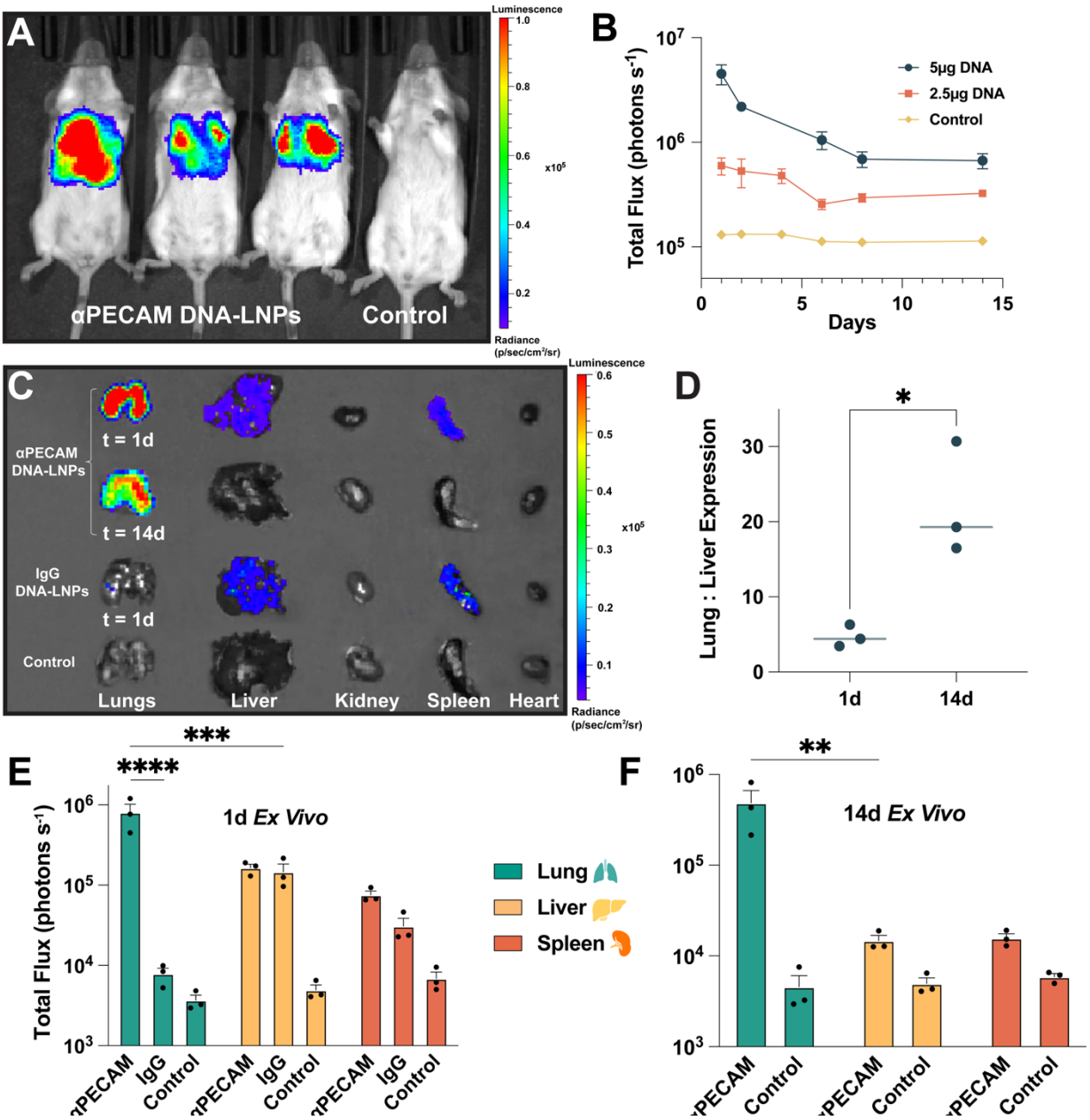

Figure 2. PECAM-targeted DNA-LNPs express in the lungs with increasing lung specificity over time. (A) Representative bioluminescence (IVIS) image of BALB/c mice treated with 5µg of luciferase pDNA loaded into αPECAM DNA-LNPs alongside a naive, luciferin-treated control shows a strong luminescent signal in the thoracic region, and notably the lobes of the lungs, at 1d. (B) Quantified total luminescence (represented as total flux in photons s^{-1}) in the area of visible signal from IVIS images over time for mice treated with 5µg and 2.5µg of pDNA loaded into αPECAM DNA-LNPs compared to naive, luciferin-treated control. The expression of luciferase is dose-dependent and plateaus by day 7. (C) Representative *ex vivo* IVIS image of major thoracic and abdominal organs from mice treated with αPECAM DNA-LNPs or IgG DNA-LNPs next to control organs from a naive, luciferin-treated mouse. Notably, luminescence is retained in the lungs at 14d and is greatly diminished in the liver. (D) Lung-to-liver ratios of *ex*

vivo luminescence underscore increasing lung specificity of expression over time from day 1 to day 14. (E & F) *Ex vivo* quantification of lung, liver, and spleen luminescence for mice treated with 5μg pDNA at 1d and 14d, respectively, shows strong retention of lung luminescence over time with marked decreases in liver and spleen signal over the same period. IgG DNA-LNP luminescence dropped to ~2x background by day 3 and was thus excluded at day 14 in panel F. For panel (D), an unpaired *t*-test with Welch's correction was performed. In panels (E) and (F), two-way ANOVAs with Tukey's multiple comparisons test were performed. All data include n = 3 and represent mean ± SEM; * = $p < 0.05$, ** = $p < 0.01$, *** = $p < 0.001$, **** = $p < 0.0001$.

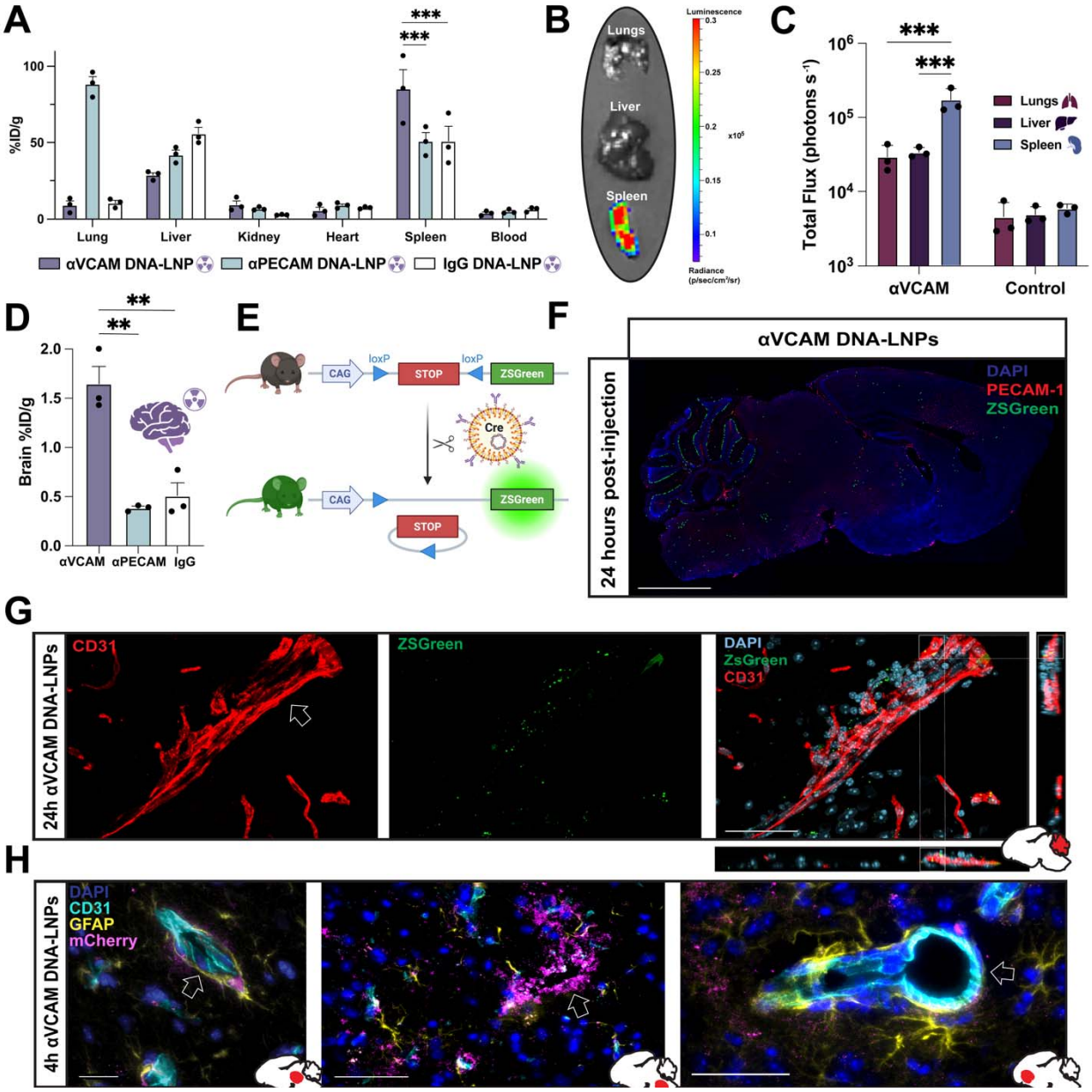

Figure 3. VCAM targeted DNA-LNPs induce elevated transgene expression in both the spleen and brain. (A) Biodistribution of αVCAM DNA-LNPs, αPECAM DNA-LNPs, and IgG DNA-LNPs via ^{125}I radiotracing in naive BALB/c mice reveals considerable shifts in particle distribution based on targeting moiety. αVCAM DNA-LNPs exhibit the highest spleen uptake compared to other particles. (B) *Ex vivo* bioluminescence imaging 1d post-injection with αVCAM DNA-LNPs containing 5μg luciferase pDNA shows the highest expression in the spleen. (C) Quantification of *ex vivo* images underscores differences in major organs of mice treated with αVCAM DNA-LNPs, exhibiting significantly higher expression in the spleen compared to both the lungs and liver. Naive, luciferin-treated controls are shown for comparison. (D) Radiotracing analysis in the brain reveals a >3x increase in particle uptake of αVCAM DNA-LNPs compared with both αPECAM and IgG DNA-LNPs. (E) Schematic depicting Cre-mediated recombination of the STOP cassette and subsequent expression of the enhanced green

fluorescent protein, ZsGreen, in Ai6 mice treated with αVCAM DNA-LNPs loaded with pDNA encoding Cre recombinase. (F) Immunofluorescent (IF) sagittal brain section (20X resolution) 24 hours after treatment with αVCAM DNA-LNPs loaded with pDNA encoding Cre recombinase. Merge depicts DAPI (blue), ZsGreen dot render (green), PECAM-1 (red) (scale bar, 1mm). (G) 60X images highlighting endothelial cells (CD31) and ZsGreen signal demonstrating colocalization of ZsGreen expression in endothelial cells and surrounding neurovasculature (scale bar, 50µm). (H) 40X IF images from the brain of a naive BALB/c mouse 4 hours after treatment with αVCAM DNA-LNPs loaded with mCherry pDNA. Merge shows DAPI (blue), CD31 (cyan), mCherry (magenta), and astrocyte marker GFAP (yellow) (scale bars, 50µm). mCherry expression is apparent in the perivascular space. For panels (G) and (H), arrows indicate blood vessels. For panels (A) and (C), two-way ANOVAs with Tukey's multiple comparisons test were performed. In panel (D), a one-way ANOVA with Tukey's multiple comparisons test was performed. All data include n = 3 and represent mean ± SEM; ** = $p < 0.01$, *** = $p < 0.001$.

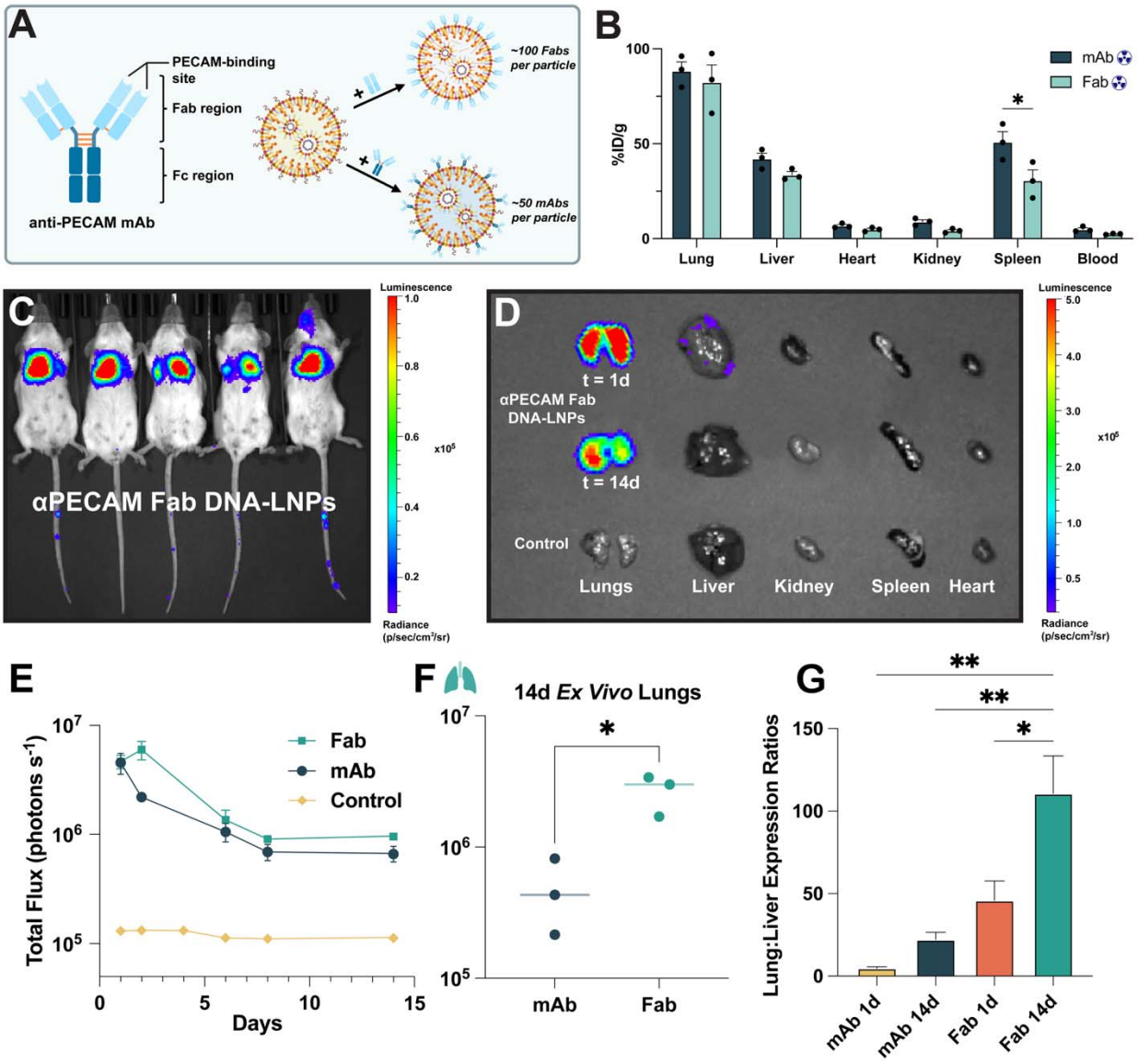

Figure 4. Conjugating anti-PECAM Fabs to DNA-LNPs immensely increases both lung specificity and expression. (A) Schematic illustrating the structure and conjugation of αPECAM mAbs vs Fabs to DNA-LNPs. Notably, Fabs are ~50 kDa compared to mAbs (~150 kDa), and lack the fragment crystallizable (Fc) region of full-length antibodies. (B) Biodistribution via radiotracing of ^{125}I-labeled Fab and mAb αPECAM DNA-LNPs reveals similar lung accumulation by both particles, and decreased uptake of Fab DNA-LNPs in the spleen. (C) Representative IVIS image of BALB/c mice treated with 5μg of luciferase pDNA loaded into αPECAM Fab DNA-LNPs shows strong luminescent signal in the thoracic cavity, especially in the lungs. (D) Representative *ex vivo* image displaying lung luminescence from αPECAM Fab DNA-LNP-treated mice that persists over time. (E) Comparison of *in vivo* luminescence shows superiority of αPECAM Fab DNA-LNPs compared to mAb DNA-LNPs. (F) *Ex vivo* quantification confirms superior lung expression at 14d in Fab condition, showing roughly an

order of magnitude increase in luminescence compared with mAb DNA-LNPs at the same time point. (G) Lung-to-liver expression ratios quantified at 1d and 14d via *ex vivo* luminescence show increasing lung specificity by αPECAM Fab DNA-LNPs over time, and overall higher ratios compared to αPECAM mAb DNA-LNPs. In panel (B), a two-way ANOVA with Tukey's multiple comparisons test was performed. For panel (F), an unpaired *t*-test with Welch's correction was performed. In panel (G), a one-way ANOVA with Tukey's multiple comparisons test was performed. All data include n = 3 and represent mean ± SEM; * = $p < 0.05$, ** = $p < 0.01$.

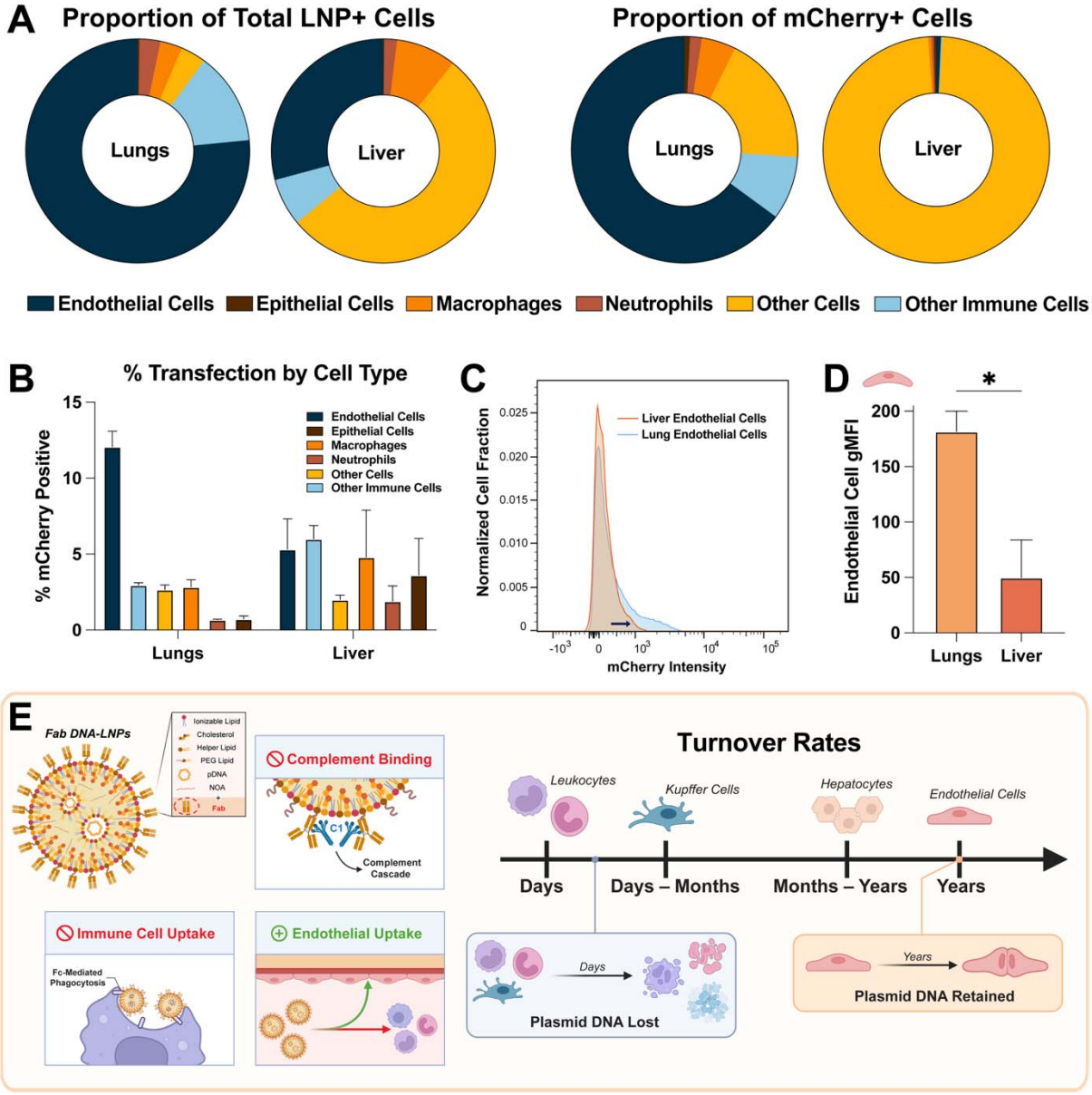

Figure 5. Anti-PECAM Fabs facilitate uptake and transgene expression of DNA-LNPs with specificity to lung endothelial cells. (A) Flow cytometry analysis tracking the (left) proportion of cells positive for fluorescent αPECAM-Fab DNA-LNPs and (right) proportion of cells positive for mCherry pDNA expression induced by αPECAM-Fab DNA-LNPs. Left panel: >75% of LNP+ cells in the lungs are endothelial (CD45-/CD31+), while the majority of LNP+ cells in the liver are "other cells" (CD45-/CD31-/EpCAM-). Right panel: mCherry pDNA transgene expression by cell type reveals that the majority of mCherry-expressing cells are endothelial in the lungs and "other cells" in the liver. Note that hepatocytes in the liver were not specifically stained for and thus fall under the "other cells" population. (B) Alternative view of the data presented in (A, right panel) showing the percentage of mCherry+ cells in each cell type in the lungs and liver, revealing the highest fraction of mCherry positivity to be in lung endothelial cells (ECs). (C) Comparison of total mCherry fluorescence in the ECs of the liver

and lungs, illustrating a significant shift in mCherry expression in lung ECs. (D) Quantification of mCherry fluorescence in lung and liver endothelial cells by geometric mean fluorescence intensity (gMFI), demonstrating significantly higher expression in lung ECs compared to liver ECs. (E) Graphic illustrating the leading hypothesis for superior lung specificity of αPECAM-Fab DNA-LNPs and increasing lung specificity over time. Left: Fabs, which lack the Fc domain of full-length mAbs, avoid classical pathway complement activation and engagement with Fc receptors on immune cells, resulting in superior lung EC binding and expression compared to mAbs[35-37]. Right: Lung ECs maintain persistent transgene expression over time due to their slower turnover rate, while more short-lived cells in the liver lose plasmid DNA and thus expression[38-40]. Additionally, turnover mechanisms affect whether pDNA is destroyed, as in apoptosis, or diluted, as in cell division. For panel (D), an unpaired *t*-test with Welch's correction was performed. All data include n = 3 and represent mean ± SEM; * = $p < 0.05$.

5. Experimental Section

Antibodies: Anti-mouse-PECAM-1/CD31 (clone 390) monoclonal antibodies and fragment antigen-binding regions were obtained from Sino Biological. Control rat IgG was purchased from Invitrogen. Anti-mouse-VCAM-1 (clone MK2.7) was produced by culturing hybridoma cells, purified using protein G sepharose (GE Healthcare Bio-Sciences, Pittsburgh, PA) and dialyzed in PBS.

Antibody modification: Antibodies (mAbs and Fabs) were functionalized with DBCO (Dibenzocyclooctyne) for conjugation to DNA-LNPs by mixing the antibody with a 7-fold molar excess of DBCO-PEG4-NHS Ester (BroadPharm) and a 0.5 molar excess of Alexa Fluor 594 NHS Ester (Thermo Fisher) for 1 hour at room temperature with rotation. Unreacted DBCO and fluorophore was removed by washing three times with 10x excess PBS in 10 kDa molecular weight cut off Amicon Ultra centrifugal filters (MilliporeSigma).

Preparation of mRNA/DNA-LNPs: Lipids (Echelon Biosciences for ionizable lipids, Avanti Polar Lipids for others), dissolved in ethanol, were combined in the molar percentages described in **Figure 1A or Figure S2**. 9(10)-nitrooleic acid (NOA) (Echelon Biosciences), dissolved in ethanol, was added to the lipid mixture at a drug-to-total lipid ratio of 0.2 (mole-to-mole). Plasmid DNA (Aldeveron) was dissolved in buffer (50 mM citrate buffer, pH 4). LNPs were formulated using microfluidics (NanoAssemblr Ignite, Precision Nanosystems) at a total flow rate of 6 mL/min, a flow rate ratio of 1:3 (lipid:nucleic acid mixture), and total lipid: nucleic acid ratio of 40-to-1 (wt/wt). Following formation, LNPs were dialyzed with 1x PBS in a 10 kDa molecular weight cut-off cassette (Life Technologies) for 2 hours.

LNP Characterization: Following formulation, nanoparticle size and polydispersity index (PDI) was measured via dynamic light scattering (DLS) using the Zetasizer Nano ZS (Malvern Instruments Ltd) The encapsulation efficiency and concentrations of pDNA within the LNPs were determined using a Quant-iT PicoGreen dsDNA assay (Invitrogen).

Antibody Radiolabeling: Rat IgG isotype control antibodies (Invitrogen) were radiolabeled with $Na^{125}I$ using Pierce's Iodogen radiolabeling method. To summarize, tubes were coated with 100μg Iodogen. IgG (at a concentration of between 1–2 mg/mL) and $Na^{125}I$ (0.25 μCi/μg protein) were incubated for 5 mins on ice. Unreacted materials were purified using 7 kDa Zeba desalting columns (Thermo Fisher Scientific). Thin-layer chromatography was used to confirm that all antibodies had >90% radiochemical purity prior to use.

Antibody Conjugation: Before conjugation, the particle concentration of azide-functionalized DNA-LNPs were measured via nanoparticle tracking analysis (NTA) using a Nanosight NS300 (Malvern Panalytical). DNA-LNPs were then incubated with DBCO-modified antibodies at the appropriate Ab:LNP ratio overnight at 4°C. Unbound antibodies were purified from the conjugation by passing the mixture through a size exclusion column loaded with Sepharose CL-4B (Cytiva). Conjugation efficiency was quantitatively assessed by measuring the ratio of the area under the curve for the fluorescent or radiolabeled antibody in the LNP peak (6–8 mL) to

the signal in the entire 24 mL elution. The conjugation efficiency for targeted LNPs range between 70-95%, depending on LNP and antibody batch, resulting in approximately 50 mAb/LNP or 100 Fabs/LNP.

Animals: All animal experiments strictly adhered to the guidelines established in the Guide for the Care and Use of Laboratory Animals (National Institutes of Health). Euthanasia techniques will strictly follow the AVMA Guidelines for the Euthanasia of Animals: 2020 Edition. Approval for all animal procedures was obtained from the University of Pennsylvania Institutional Animal Care and Use Committee. Naive BALB/c and B6.Cg-Gt(ROSA)26Sortm6(CAG-ZsGreen1)Hze (Ai6 for short) mice aged 6–8 weeks weighing 18–25 g, were procured from The Jackson Laboratory for all studies. The mice were housed in a controlled environment run by the University Laboratory Animal Resources (ULAR) facility and were maintained at temperatures between 22 °C and 26 °C with a 12-h light/dark cycle, and provided with ample access to food and water.

In Vivo Studies: For *in vivo* studies, although our LNPs do not produce unacceptably high levels of distress, the following guidelines were strictly adhered to by euthanizing all animals that met any of the following criteria: 1. Animals have a body condition score of 1; 2. Animals have a body condition score of 2 in addition to other signs of distress such as hunched posture, porphyrin staining, inactivity, ruffled hair coat, or dehydration; 3. Animals show overt signs of injury (redness, swelling); 4. Animals show weight loss >= 20%. All intravenous (IV) injections were done retro-orbitally by injecting into the retro-bulbar sinus. All euthanizations were performed using both cervical dislocation and exsanguination by cutting the IVC and descending aorta.

Biodistribution Studies: For biodistribution studies, $Na^{125}I$ IgG was conjugated to LNPs at a ratio of 5 IgG/LNP as a signal to track particle distribution, alongside the targeted or control antibody at the usual 50 mAb/LNP or 100 Fab/LNP. Following Antibody-LNP conjugation and purification, mice were IV injected with LNPs at a dose of approximately 2.5µg DNA. Thirty minutes after injection, animals were sacrificed. Blood was collected in EDTA-coated tubes (Thermo Fisher), and organs (lung, liver, spleen, heart, kidney, and brain) were collected and weighed. Tissue distribution of injected materials was determined by measuring the radioactivity in the blood and organs using a Wizard 2470 Gamma Counter (PerkinElmer). Organ uptake was calculated as percent injected dose normalized to the mass of tissue (%ID/g tissue).

In Vivo Imaging System (IVIS) for Luciferase Expression: Prior to IVIS imaging, mice were intravenously injected with targeted or control DNA-LNPs loaded with pDNA encoding for Luciferase (Aldevron) at a dose of 2.5 or 5µg. 1-14 days post treatment, mice were put under using 3% isoflurane-induced and intraperitoneally injected with 100µl of 30 mg/mL D-luciferin sodium salt (Regis Technologies). Anesthetized mice were placed in an IVIS Spectrum machine (Revvity) face up (to view the thorax) and imaged for chemiluminescence in the target area every minute with automatically determined exposure time for 10–14 images, until the signal reached the peak intensity. Revvity LivingImage software (version 4.8.2) was used to analyze images.

Ex Vivo Imaging: Following IVIS imaging on either day 1 or 14, mice that were already intraperitoneally injected with 100µl of 30 mg/mL D-luciferin sodium salt (Regis Technologies) were anesthetized and euthanized. Organs (lungs, liver, spleen, heart, kidney, and brains) were collected, organized on a sheet, and imaged for chemiluminescence in an IVIS Spectrum machine (Revvity). Revvity LivingImage software (version 4.5.5) was used to analyze images.

Flow Cytometry: Naive mice were intravenously injected with either αPECAM-Fab DNA-LNPs formulated with 0.3% DSPE-PEG-Fluor 488 (Broad Pharm), to track particle delivery, or normal αPECAM-Fab DNA-LNPs loaded with pDNA encoding mCherry (Aldevron). Either 30 minutes (fluorescent LNPs) or 24 hours (mCherry LNPs) after treatment, mice were euthanized and transcardially perfused with PBS to clear blood and preserve tissue. The lungs and liver of the mice were collected and triturated before being incubated in a digestive solution of 2 mg/mL type 1 collagenase (Gibco) and 100µL of 2.5 mg/mL DNAse (Roche) for 45 min to prepare a single-cell suspension. After incubation, the cells were strained through a 70µm cell strainer (Sycamore Life Science) and washed with PBS. The supernatant was discarded, and ACK lysis buffer (Gibco) was added for 5 min on ice to lyse any remaining red blood cells (RBCs). After RBC lysis, an automated cell counter (Countess, Thermo Fisher) was used to achieve a final cell concentration of 1×10^6 cells/mL for each sample. Suspensions were washed with Fluorescence-activated Cell Sorting (FACS) buffer, consisting of PBS, 1% Fetal Bovine Serum (FBS, Thermo Fisher Scientific), and 1 mM Ethylenediaminetetraacetic Acid (EDTA, Invitrogen) and incubated with anti-CD16/CD32 monoclonal antibodies (Invitrogen) for 15 minutes to prevent nonspecific binding of antibodies on Fc-receptors. Following washing, suspensions were incubated for another 30 mins with an antibody cocktail consisting of brilliant ultra violet (BUV) 395 anti-mouse CD45, clone: 30-F11 (BD Biosciences), phycoerythrin (PE)/cyanine7 anti mouse-CD64, clone: FcγRI (BioLegend), and alexa fluor 700 anti-mouse Ly6G, clone: Gr-1 (BioLegend) to identify immune cell subpopulations and allophycocyanin (APC) anti-mouse CD31 (BioLegend) and brilliant violet 711 (BV711) anti-mouse Ep-CAM, clone:CD326 (BioLegend) for endothelial and epithelial cells. After antibody incubation, the cells were fixed with 4% paraformaldehyde (PFA, Electron Microscopy Sciences) before analysis on a flow cytometer (LSR Fortessa, BD BioSciences). Gating parameters for analysis are illustrated in **Figure S8**. The flow cytometry results were analyzed using FlowJo™ Software v10.10 (BD Life Sciences).

Histology: Either naive BALB/c or B6.Cg-Gt(ROSA)26Sortm6(CAG-ZsGreen1)Hze (Ai6 for short) mice were intravenously injected with targeted DNA-LNPs (conjugated to either αPECAM Fabs for lung histology or αVCAM mAbs for brain histology) loaded with pDNA (Aldevron) encoding mCherry 4 hours or Cre recombinase 24 hours prior to perfusion. For brain histology, mice were perfused through the left ventricle (after cutting the right atrium) with 15mL 1x PBS followed by 15mL 4% PFA (EMS). For lung histology, mice were perfused with 10mL 1x PBS through the right ventricle at 20cm H2O, the trachea was sutured shut, and the lungs were inflated with 4% PFA by injection into the trachea. Organs were then drop-fixed in 4% PFA for 16-24 hours at 4 degrees C and then cryo-protected in 30% sucrose (Neta Scientific) for at least 48 hours, embedded in OCT (Fisher), cryo-sectioned at 16um or 35um (in the case of lung confocal microscopy), mounted on Superfrost Plus slides (Fisher), and frozen at −80 degrees C. Slides were then thawed at 60 degrees C, rehydrated in 1x PBS, and blocked for one hour at RT in blocking buffer - 90% 1x PBS, 9.5% donkey serum (Sigma), 0.5% Triton X-100 (Sigma). After blocking, slides were incubated with primary antibodies (described below) in

staining buffer (98.5% 1x PBS, 1% donkey serum, 0.5% Triton X-100) overnight at 4 degrees C. In the morning, slides were washed with 1x PBS and incubated with secondary antibodies (described below) for one hour at RT in staining buffer. Slides were washed once more and coverslipped with DAPI mounting media (EMS) before imaging. Controls at identical exposure settings for both lung and brain histology are shown in **Figure S7**.

Antibodies used: Goat Anti-CD31(Biotechne, 1:400); Rabbit Anti-Iba1 (Fujifilm, 1:600); Rat Anti-GFAP (Agilent, 1:400); Guinea pig Anti-S100B (BD Biosciences, 1:400); Chicken polyclonal Anti-mCherry (Abcam, 1:200); Donkey anti-goat IgG 488, 647 (ThermoFisher, 1:500); Donkey anti-rabbit IgG 594, 647 (ThermoFisher, 1:500); Donkey anti-rat IgG 488 (ThermoFisher, 1:500) Donkey anti-chicken 647 (ThermoFisher, 1:500); Donkey anti-guinea pig 647 (BD biosciences, 1:500).Microscopes used: BZ-x800 widefield fluorescent microscope and Andor benchtop confocal microscope. Fiji and Imaris softwares used for image processing and analysis.

Microscopes used: BZ-x800 widefield fluorescent microscope and Andor benchtop confocal microscope. Fiji and Imaris softwares used for image processing and analysis. Dot render generation implemented Fiji software to threshold, create masks, and circularize masks into dot signals which were overlaid onto the composite image for improved visualization as done previously[44].

Statistics: Statistical analyses were performed using GraphPad Prism 10 (GraphPad Software). All data include n = 3 and represent mean ± SEM; * = $p < 0.05$, ** = $p < 0.01$, *** = $p < 0.001$, **** = $p < 0.0001$. The statistical test(s) used for any experiment is described in each corresponding figure.

Acknowledgments: N.M. and T.V.B. contributed equally to this work. Research reported in this publication was supported by the National Science Foundation under Cooperative Agreement DBI – 2400327 (to T.V.B. and V.R.M.), the National Center for Advancing Translational Sciences of the National Institutes of Health- KL2TR001879 (to E.E.), National Library of Medicine under the National Institutes of Health- R01NS131279 (For O.A.M.C.), the National Institute of Health- 1DP5OD036159 (for M.L.B.), R01-HL-153510 (J.S.B.), -HL160694 (J.S.B.), -HL164594, (J.S.B.), -HL-157189 (J.S.B.), -HL-155106 (V.R.M.) and the American Heart Association under grant 24PRE1195406 (to M.N.P.). The flow cytometry data for this manuscript were generated in the Penn Cytomics and Cell Sorting Shared Resource Laboratory at the University of Pennsylvania (RRID:SCR_022376). Penn Cytomics is partially supported by the Abramson Cancer Center NCI Grant (P30 016520). The content is solely the responsibility of the authors and does not necessarily represent the official views of the National Institutes of Health.

6. Citations

1. Hou, X., Zaks, T., Langer, R. & Dong, Y. Lipid nanoparticles for mRNA delivery. *Nature Reviews Materials* **6**, 1078-1094 (2021).

2. Swetha, K. et al. Recent Advances in the Lipid Nanoparticle-Mediated Delivery of mRNA Vaccines. *Vaccines (Basel)* **11** (2023).
3. Kalita, T., Dezfouli, S.A., Pandey, L.M. & Uludag, H. siRNA Functionalized Lipid Nanoparticles (LNPs) in Management of Diseases. *Pharmaceutics* **14** (2022).
4. Kimura, S., Khalil, I.A., Elewa, Y.H.A. & Harashima, H. Novel lipid combination for delivery of plasmid DNA to immune cells in the spleen. *J Control Release* **330**, 753-764 (2021).
5. Cheng, Z. et al. The interactions between cGAS-STING pathway and pathogens. *Signal Transduct Target Ther* **5**, 91 (2020).
6. Patel, M.N. et al. Safer non-viral DNA delivery using lipid nanoparticles loaded with endogenous anti-inflammatory lipids. *Nature Biotechnology* (2025).
7. Hansen, A.L. et al. Nitro-fatty acids are formed in response to virus infection and are potent inhibitors of STING palmitoylation and signaling. *Proceedings of the National Academy of Sciences* **115**, E7768-E7775 (2018).
8. Grieger, J.C. & Samulski, R.J. Packaging capacity of adeno-associated virus serotypes: impact of larger genomes on infectivity and postentry steps. *J Virol* **79**, 9933-9944 (2005).
9. George, L.A. et al. Long-Term Follow-Up of the First in Human Intravascular Delivery of AAV for Gene Transfer: AAV2-hFIX16 for Severe Hemophilia B. *Mol Ther* **28**, 2073-2082 (2020).
10. Mingozzi, F. & High, K.A. Immune responses to AAV vectors: overcoming barriers to successful gene therapy. *Blood* **122**, 23-36 (2013).
11. Liu, W. et al. Understanding Atherosclerosis Through an Osteoarthritis Data Set. *Arterioscler Thromb Vasc Biol* **39**, 1018-1025 (2019).
12. Di, J. et al. Biodistribution and Non-linear Gene Expression of mRNA LNPs Affected by Delivery Route and Particle Size. *Pharm Res* **39**, 105-114 (2022).
13. Evans, C.E., Cober, N.D., Dai, Z., Stewart, D.J. & Zhao, Y.Y. Endothelial cells in the pathogenesis of pulmonary arterial hypertension. *Eur Respir J* **58** (2021).
14. Kleeberg, A., Luft, T., Golkowski, D. & Purrucker, J.C. Endothelial dysfunction in acute ischemic stroke: a review. *J Neurol* **272**, 143 (2025).
15. Wei, H. et al. Characterization of the polarized endothelial secretome. *Faseb j* **33**, 12277-12287 (2019).
16. Wang, S. et al. Unleashing the Potential: Designing Antibody-Targeted Lipid Nanoparticles for Industrial Applications with CMC Considerations and Clinical Outlook. *Mol Pharm* **21**, 4-17 (2024).
17. LoPresti, S.T., Arral, M.L., Chaudhary, N. & Whitehead, K.A. The replacement of helper lipids with charged alternatives in lipid nanoparticles facilitates targeted mRNA delivery to the spleen and lungs. *J Control Release* **345**, 819-831 (2022).
18. He, Y. et al. Development of a Combined Lipid-Based Nanoparticle Formulation for Enhanced siRNA Delivery to Vascular Endothelial Cells. *Pharmaceutics* **14** (2022).
19. Zamora, M.E. et al. Combination of Physicochemical Tropism and Affinity Moiety Targeting of Lipid Nanoparticles Enhances Organ Targeting. *Nano Letters* **24**, 4774-4784 (2024).
20. Omo-Lamai, S. et al. Physicochemical Targeting of Lipid Nanoparticles to the Lungs Induces Clotting: Mechanisms and Solutions. *Advanced Materials* **36**, 2312026 (2024).

21. Scherpereel, A. et al. Platelet-endothelial cell adhesion molecule-1-directed immunotargeting to cardiopulmonary vasculature. *J Pharmacol Exp Ther* **300**, 777-786 (2002).
22. Howard, M. et al. Vascular targeting of nanocarriers: perplexing aspects of the seemingly straightforward paradigm. *ACS Nano* **8**, 4100-4132 (2014).
23. Parhiz, H. et al. PECAM-1 directed re-targeting of exogenous mRNA providing two orders of magnitude enhancement of vascular delivery and expression in lungs independent of apolipoprotein E-mediated uptake. *J Control Release* **291**, 106-115 (2018).
24. Singh, V., Kaur, R., Kumari, P., Pasricha, C. & Singh, R. ICAM-1 and VCAM-1: Gatekeepers in various inflammatory and cardiovascular disorders. *Clin Chim Acta* **548**, 117487 (2023).
25. Marcos-Contreras, O.A. et al. Selective targeting of nanomedicine to inflamed cerebral vasculature to enhance the blood-brain barrier. *Proc Natl Acad Sci U S A* **117**, 3405-3414 (2020).
26. Nong, J. et al. Targeting lipid nanoparticles to the blood-brain barrier to ameliorate acute ischemic stroke. *Mol Ther* **32**, 1344-1358 (2024).
27. Corroyer-Dulmont, A. et al. VCAM-1 targeted alpha-particle therapy for early brain metastases. *Neuro Oncol* **22**, 357-368 (2020).
28. Reyes-Esteves, S. et al. Targeted drug delivery to the brain endothelium dominates over passive delivery via vascular leak in experimental intracerebral hemorrhage. *J Control Release* **356**, 185-195 (2023).
29. Zhang, L. et al. Effect of mRNA-LNP components of two globally-marketed COVID-19 vaccines on efficacy and stability. *NPJ Vaccines* **8**, 156 (2023).
30. Zaleski, M.H. et al. Conjugation Chemistry Markedly Impacts Toxicity and Biodistribution of Targeted Nanoparticles, Mediated by Complement Activation. *Adv Mater* **37**, e2409945 (2025).
31. Gosk, S., Moos, T., Gottstein, C. & Bendas, G. VCAM-1 directed immunoliposomes selectively target tumor vasculature in vivo. *Biochim Biophys Acta* **1778**, 854-863 (2008).
32. Bates, A. & Power, C.A. David vs. Goliath: The Structure, Function, and Clinical Prospects of Antibody Fragments. *Antibodies (Basel)* **8** (2019).
33. Nimmerjahn, F. & Ravetch, J.V. Fcgamma receptors as regulators of immune responses. *Nat Rev Immunol* **8**, 34-47 (2008).
34. Liu, R., Oldham, R.J., Teal, E., Beers, S.A. & Cragg, M.S. Fc-Engineering for Modulated Effector Functions-Improving Antibodies for Cancer Treatment. *Antibodies (Basel)* **9** (2020).
35. Kang, T.H. & Jung, S.T. Boosting therapeutic potency of antibodies by taming Fc domain functions. *Exp Mol Med* **51**, 1-9 (2019).
36. Tay, M.Z., Wiehe, K. & Pollara, J. Antibody-Dependent Cellular Phagocytosis in Antiviral Immune Responses. *Front Immunol* **10**, 332 (2019).
37. Zamora, M.E. et al. Marginated Neutrophils in the Lungs Effectively Compete for Nanoparticles Targeted to the Endothelium, Serving as a Part of the Reticuloendothelial System. *ACS Nano* **18**, 22275-22297 (2024).
38. Montezano, A.C., Neves, K.B., Lopes, R.A. & Rios, F. Isolation and Culture of Endothelial Cells from Large Vessels. *Methods Mol Biol* **1527**, 345-348 (2017).

39. Patel, A.A., Ginhoux, F. & Yona, S. Monocytes, macrophages, dendritic cells and neutrophils: an update on lifespan kinetics in health and disease. *Immunology* **163**, 250-261 (2021).
40. Duncan, A.W., Dorrell, C. & Grompe, M. Stem cells and liver regeneration. *Gastroenterology* **137**, 466-481 (2009).
41. Bhandari, S., Larsen, A.K., McCourt, P., Smedsrød, B. & Sørensen, K.K. The Scavenger Function of Liver Sinusoidal Endothelial Cells in Health and Disease. *Front Physiol* **12**, 757469 (2021).
42. Øie, C.I. et al. Liver sinusoidal endothelial cells contribute to the uptake and degradation of entero bacterial viruses. *Sci Rep* **10**, 898 (2020).
43. Furman, D. et al. Chronic inflammation in the etiology of disease across the life span. *Nat Med* **25**, 1822-1832 (2019).
44. Chadarevian, J.P., Davtyan, H., Lombroso, S.I., Bennett, F.C. & Blurton-Jones, M. CRISPR generation of CSF1R-G795A human microglia for robust microglia replacement in a chimeric mouse model. *STAR Protoc* **4**, 102490 (2023).